Mineralium Deposita (2019) 54:1265–1280
https://doi.org/10.1007/s00126-019-00875-7

ARTICLE

Two episodes of REE mineralization in the Qinling Orogenic Belt, Central China: in-situ U-Th-Pb dating of bastnäsite and monazite

Wei Zhang[1] · Wei Terry Chen[1,2] · Jian-Feng Gao[1] · Hua-Kai Chen[3] · Jing-Hui Li[3]

Received: 10 October 2018 / Accepted: 11 March 2019 / Published online: 30 March 2019

Abstract

Recent exploration revealed a number of rare earth element (REE) deposits that are distributed along the Qinling Orogenic Belt, Central China. These deposits have an estimated total reserve of about 2 Mt. REE_2O_3, thus making this belt a world-class REE metallogenic province. Understanding the metallogenesis of the belt requires direct dating of REE minerals. In this study, LA-ICP-MS U-Th-Pb dating on bastnäsite and monazite from the Huangshuian, Taipingzhen, and Miaoya deposits in different units of the belt was used to precisely determine the timing of the REE mineralization. The Huangshuian deposit in the north is a carbonatite-related Mo-(REE) deposit in which the REE minerals are closely associated with molybdenite. After correction for common Pb and excessed ^{206}Pb decayed from ^{230}Th, a weighted average $^{206}Pb/^{238}U$ age of 207 ± 4 Ma (n = 17; MSWD = 1.9) is obtained for bastnäsite grains from this deposit. Such an age is slightly younger than that of the final collision (peak at 230–220 Ma) of the Qinling Orogenic Belt, thus indicating that the Mo-REE mineralization is likely related to a post-collisional extension setting. The Taipingzhen REE deposit in the middle contains sheet-like ore bodies composed of veins where bastnäsite, the dominant REE mineral, is closely associated with quartz, fluorite, and barite. In situ bastnäsite U-Th-Pb dating shows that the REE mineralization in this deposit has formed at 421 ± 7 Ma (n = 17; MSWD = 1.5), synchronous with extension-related magmatism in the region. The Miaoya deposit in the south is the largest one in the belt, and it is essentially a REE-mineralized syenite-carbonatite complex. In this deposit, the monazite grains are closely associated with major minerals of the syenites or carbonatites (e.g., K-feldspar or calcite), but commonly exhibit complex internal textures. Different domains of monazite yield two groups of U-Pb ages at 414 ± 11 Ma (n = 5; MSWD = 0.91) and 231 ± 2 Ma (n = 21; MSWD = 3.1), whereas the bastnäsite has an age of 206 ± 4 Ma (n = 14; MSWD = 1.5). The early age of 414 Ma is obtained from homogenous monazite grains and in good agreement with zircon U-Pb ages of the Miaoya syenite-carbonatite complex, and thus is considered to represent the timing of the major REE mineralization in the deposit. The younger ages of 231–206 Ma are obtained from monazite grains with complex internal textures and bastnäsite in late veinlets, thus recording secondary, consecutive REE remobilization events likely related to the compression process during formation of the Qinling Orogenic Belt. Our new U-Th-Pb ages, in combination with previously geochronological data, demonstrate that there are two episodes of REE mineralization at 440–410 Ma and 220–200 Ma in the Qinling Orogenic Belt.

Keywords Qinling · REE deposit · Bastnäsite · Monazite · U-Th-Pb age

Editorial handling: R. Linnen

Electronic supplementary material The online version of this article (https://doi.org/10.1007/s00126-019-00875-7) contains supplementary material, which is available to authorized users.

✉ Wei Terry Chen
chenwei@mail.gyig.ac.cn

[1] State Key Laboratory of Ore Deposit Geochemistry, Institute of Geochemistry Chinese Academy of Sciences, Guiyang 550081, China

[2] University of Chinese Academy of Sciences, Beijing 10039, China

[3] Henan Nuclear Geological Bureau, Zhengzhou 450044, China

Introduction

The Qinling Orogenic Belt is located in central China and links North China Craton in the north with South China Craton in the south (Fig. 1a). Recent exploration revealed a number of rare earth element (REE) and REE-bearing deposits that are suggested to be carbonatite-related. Typical examples include the Miaoya and Shaxiongdong REE-Nb deposits in the south, Huangshuian and Huanglongpu Mo-(REE) deposits, Huayangchuan U-Nb-Pb-REE deposit in the north, and the newly discovered Taipingzhen REE deposit in the middle

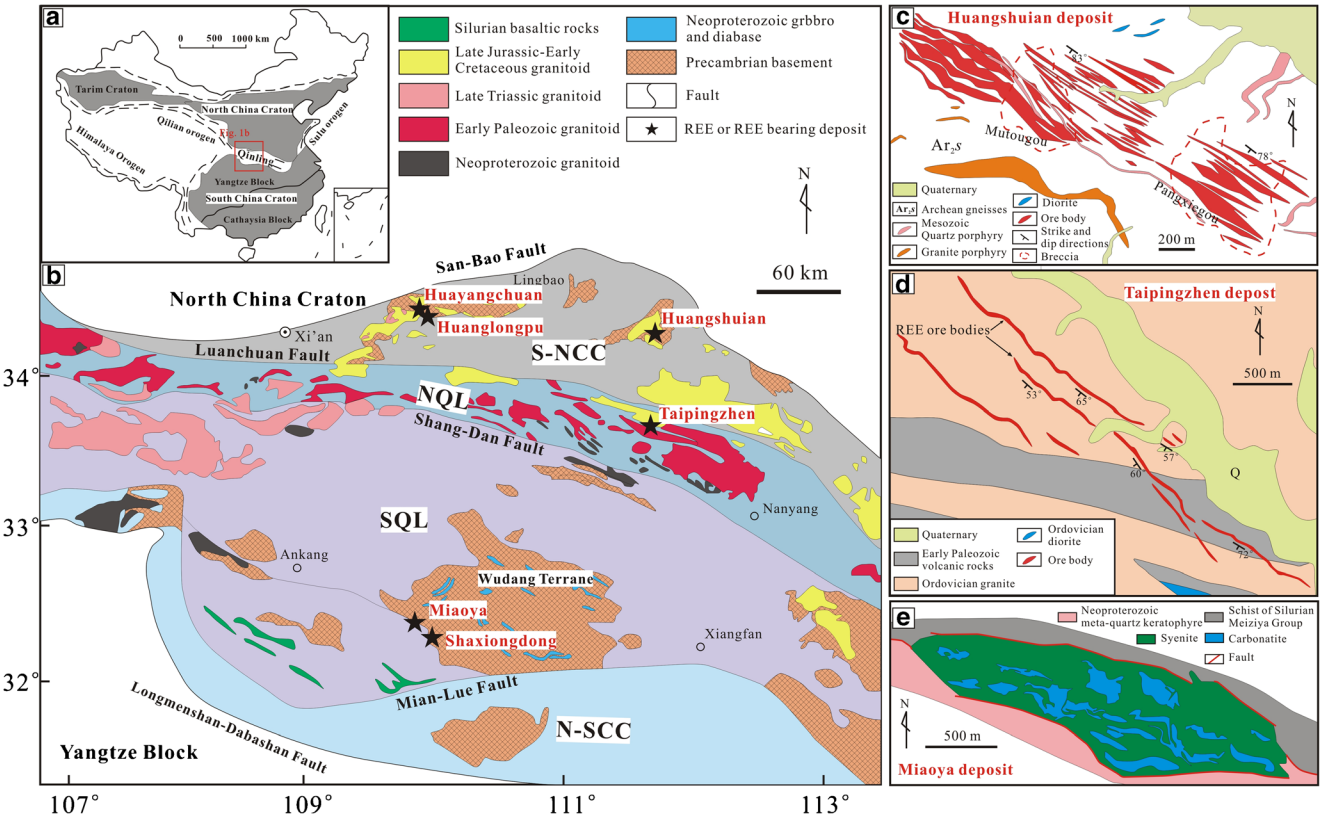

Fig. 1 **a** Tectonic map of China. **b** Geological sketch of the Qinling Orogenic Belt. Also shown is the location of REE and REE-bearing deposits. **c** Simplified geological map of the Huangshuian Mo-(REE) deposit (modified from Cao et al. 2014). **d** Simplified geological map of the Taipingzhen REE deposit (modified from Li et al. 2017). **e** Simplified geological map of the Miaoya REE-Nb deposit (modified from Xu et al. 2014). Abbreviations: S-NCC: Southern North China Craton, NQL: North Qinling unit, SQL: South Qinling unit, N-SCC: Northern South China Craton

(Fig. 1b). These deposits have an estimated total REE reserve of approximately 2 Mt. REE_2O_3 (Qian and Li 1996; Li et al. 2017; Gao et al. 2017), thus making the Qinling Orogenic Belt potentially one of the most important REE metallogenic provinces. The timing of REE mineralization in this belt has long been an important issue but is currently not comprehensively constrained. The timing of mineralization was proposed to be at ca. 220 (Stein 1997; Huang et al. 2009; Cao et al. 2014; Song et al. 2015, 2016) or ca. 440 Ma (Xu et al. 2008; Lu et al. 2014; Zhu et al. 2016; Ying et al. 2017). However, these ages were mostly obtained by indirect dating of associated host rocks (e.g., carbonatite or syenite) or minerals associated with REE minerals in the ores, such as zircon U-Pb and Molybdenite Re-Os ages (e.g., Stein 1997; Huang et al. 2009; Cao et al. 2014; Song et al. 2015; Zhu et al. 2016). It is unclear if the REE mineralization is genetically related to the host rocks or if it is synchronous with the Mo mineralization.

Bastnäsite and monazite are common ore minerals in REE deposits, and precisely determining their ages would provide convincing constraints on the timing and tectonic environment of the specific REE mineralization. Both minerals contain considerable concentrations of U and Th, and are thus good candidates for precise U-Th-Pb dating (Parrish 1990; Poitrasson et al. 2000; Sal'nikova et al. 2010; Ling et al. 2016). Recent development of laser ablation inductively coupled plasma mass spectrometry (LA-ICP-MS) allows in-situ analyses with high sensitivity and spatial resolution, and has been proven to be a robust tool for in-situ U-Th-Pb dating of bastnäsite and monazite, particular for minerals with complex internal textures (e.g., Simonetti et al. 2006; Paquette and Tiepolo 2007; Kosler et al. 2010; Yang et al. 2014).

In this study, detailed investigations on paragenetic relationships of the REE mineralization in the Huangshuian, Taipingzhen, and Miaoya deposits are provided. We obtained in-situ LA-ICP-MS U-Th-Pb ages of bastnäsite and monazite from these deposits, in order to constrain the timing of REE mineralization events in the Qinling Orogenic Belt. Our new dataset provides direct isotopic constraints on the timing of these deposits, and hence a better understanding of the tectonic evolution and REE metallogeny of the belt.

Regional geology

The Qinling Orogenic Belt, which is bound by the San–Bao Fault to the north and the Longmenshan–Dabashan Fault to

the south, comprises of four tectonic units that are separated by the Luanchuan, Shang-Dan, and Mian–Lue Faults from north southward, including Southern North China Craton, North Qinling unit, South Qinling unit, and Northern South China Craton (Fig. 1b). The belt has experienced complex orogenic events including the collision of North Qinling unit and South Qinling unit in the Carboniferous and the final collision of the North China Craton and South China Craton in the Triassic (Meng and Zhang 2000; Wu and Zheng 2013; Dong and Santosh 2016).

The Southern North China Craton consists mainly of Archean to Early Paleoproterozoic basement rocks overlaid by late Paleoproterozoic to Phanerozoic cover sequences (Kröner et al. 1988; Zhang et al. 2001a; Wan et al. 2006; Huang et al. 2010). The basement is dominated by the Taihua Group (2.84–1.97 Ga) that is composed of amphibolite- to granulite- facies metamorphic rocks including graphite-bearing gneisses, greenstones, biotite gneisses, marbles, and banded iron formations. The Taihua Group is unconformably overlain by the Paleoproterozoic Xiong'er Group which is composed mainly of intermediate to acidic lavas and pyroclastic rocks intercalated with minor sedimentary rocks (< 5%; Zhao et al. 2004, 2009). The Xiong'er Group is in turn unconformably overlain by Mesoproterozoic to Neoproterozoic sedimentary rocks. Mesozoic magmatic intrusions are widespread in the region and were mainly formed at 220–190 and 160–110 Ma. The former stage is characterized by alkaline rocks which are interpreted to have formed in an extensional setting (Wang et al. 2007; Ding et al. 2011; Cao et al. 2015). The latter stage of 160–110 Ma is dominated by granites and porphyries that are commonly associated with Mo mineralization (Mao et al. 2011; Li and Pirajno 2016).

The North Qinling unit is dominated by Proterozoic to Paleozoic medium to high-grade metasedimentary and metavolcanic rocks (Zhang et al. 1994; Liu et al. 2016), including Kuanping, Erlangping, Qinling, and the Danfeng Groups from north to south. The Kuanping Group is a suite of greenschist-facies meta-volcanic-sedimentary rocks with Neoproterozoic to Ordovician ages. The Erlangping Group comprises mainly of Late Paleozoic sedimentary and Early Paleozoic ophiolitic mélange units. The Paleoproterozoic Qinling Group is a medium- to high-grade metamorphic complex composed of gneisses, schists, amphibolites, marble, and calc-silicate rocks. The Danfeng Group crops out in the southern margin and is composed of arc volcanic-sedimentary rocks that underwent greenschist to low amphibolite facies metamorphism. Abundant granitoids with ages of 510–400 Ma occurred in the North Qinling unit, and their formation was suggested to be related to Paleozoic subduction of Prototethyan oceanic crust and subsequent collision and back-arc opening processes (Zhang et al. 2013; Wang et al. 2015; Abdallsamed et al. 2017; Li et al. 2018).

The South Qinling unit consists mainly of Precambrian crystalline basement covered by Sinian to Phanerozoic sedimentary rocks (Zhang et al. 2001a; Ling et al. 2008; Zhu et al. 2014). The basement rocks include the Douling and Xiaomoling Complexes, and Wudangshan and Yaolinghe Groups, all of which were metamorphosed under greenschist- to amphibolite-facies conditions. The sedimentary cover contains Sinian carbonate rocks, Cambrian-Ordovician limestones, Silurian shales, Devonian-Carboniferous clastic rocks, and minor Late Paleozoic to Early Triassic clastic sedimentary rocks. The Precambrian basement and Paleozoic strata were intruded by abundant Silurian alkaline rocks and diabase dykes which show geochemical affinities of an extension rift setting (e.g., Zhang et al. 2007; Xu et al. 2008; Zhu et al. 2016; Wang et al. 2017).

The Northern South China Craton, commonly considered as a foreland fold-and-thrust belt at the northern margin of the South China Craton, shares similar basement structures and lithostratigraphic units with the South Qinling unit (Meng and Zhang 2000). It consists mainly of highly metamorphosed Neoarchean-Paleoproterozoic crystalline and greenschist-facies metamorphosed Meso- to Neoproterozoic transitional basements, covered by non-metamorphosed Sinian-Mesozoic clastic and carbonate rocks.

REE mineralization in the Qinling Orogenic Belt

The REE and REE-bearing deposits in the Qinling Orogenic Belt are spatially associated with carbonatites and/or alkaline rocks. In Southern North China Craton, REEs are essentially by-products of carbonatite-related Mo or U deposits, such as the well-known Huangshuian and Huanglongpu Mo-(REE) deposits (Li et al. 2008; Huang et al. 2009; Xu et al. 2010; Cao et al. 2014; Kynicky et al. 2012) and Huayangchuan U-Nb-Pb-REE polymetallic deposit (Gao et al. 2017). On the other hand, the vein-type Taipingzhen deposit, which was recently discovered by Henan Nuclear Geological Bureau (Li et al. 2017), is the only reported REE deposit in the North Qinling unit. In South Qinling unit, typical examples include the Miaoya and Shaxiongdong REE-Nb deposits where the ore bodies are all hosted in carbonatite-syenite complexes. Detailed descriptions of the geology of these deposits are available in the literature (Huang et al. 2009; Xu et al. 2008, 2010, 2015; Cao et al. 2014; Li 2014; Li et al. 2017; Zhu et al. 2016, 2017; Gao et al. 2017; Ying et al. 2017; Smith et al. 2018). They are briefly summarized below by taking the Huangshuian, Taipingzhen, and Miaoya deposits as the representatives.

Huangshuian Mo-(REE) deposit

The Huangshuian Mo-(REE) deposit in Songxian county, Henan Province is located in the northern part of Southern North China Craton (Fig. 1b). This deposit contains a reserve of approximately 0.4 Mt. Mo (average grade of 0.062 wt%) with REEs as the major by-product. The Mo-(REE) ore bodies are lenticular in shape (50–1000 m long) and strike northwest with steep dips that average ~ 80°N (Fig. 1c). They are mostly hosted in carbonatites that intrude the Taihua Group (Fig. 2a), but locally some ore bodies extend into the Taihua Group. Most of the ore bodies are crosscut by quartz-calcite-sulfide stockworks of 0.1 to 4 cm in thicknesses. Breccias are locally present and are generally associated with ore bodies. They consist of clasts of carbonatites and rocks of the Taihua Group, which are cemented by hydrothermal matrix (Fig. 2b).

This deposit has a paragenetic sequence of early barren carbonatite and late hydrothermal mineralization stages. The barren carbonatite dykes are generally pink in color and composed dominantly of calcite, quartz, and K-feldspar with minor REE minerals (bastnäsite, parisite, and monazite) and disseminated molybdenite (Fig. 3a). The hydrothermal mineralization stage is characterized by abundant veins that crosscut the early carbonatites, and consist of variable amounts of quartz, calcite, barite, fluorite, fluorapatite, pyrite, galena, molybdenite, and REE minerals. The REE minerals are dominated by bastnäsite, parisite, and monazite with minor ancylite, synchysite, allanite, and xenotime. They are present as subhedral to anhedral grains that are closely associated with molybdenite (Fig. 3b).

Taipingzhen REE deposit

The Taipingzhen deposit, located at the center of the North Qinling unit, was discovered by Henan Nuclear Geological Bureau in 2014. It contains an estimated reserve of approximately 0.14 Mt. REE_2O_3 with an average grade of 2.32 wt% (Li et al. 2017). The REE ore bodies are essentially sheets composed of series of veins or veinlets, which are structurally controlled by subparallel NWW-trend faults or shear zones in the Early Paleozoic Erlangping Group and Ordovician Zhangjiazhuang granite intrusion (Fig. 1d). Carbonatites are locally present at depth, but are spatially associated with ore bodies.

The REE ores are commonly vein or veinlet-type and are composed mainly of quartz, fluorite, barite, and REE minerals with minor apatite, albite, biotite, pyrite, magnetite, molybdenite, and chalcopyrite. Contents of REE minerals in the ores are highly variable, and locally, concentrations of REE_2O_3 reach up to 15 wt% (e.g., Fig. 2c). The REE minerals are dominated by bastnäsite (~ 70%) with subordinate parisite, monazite, cerite, and allanite (Fig. 3c–f). Bastnäsite is generally euhedral and locally is replaced by parisite or allanite along the margins. Parisite is subordinate to bastnäsite, but locally highly concentrated (Fig. 3e). Monazite is euhedral and commonly present in samples where apatite is abundant.

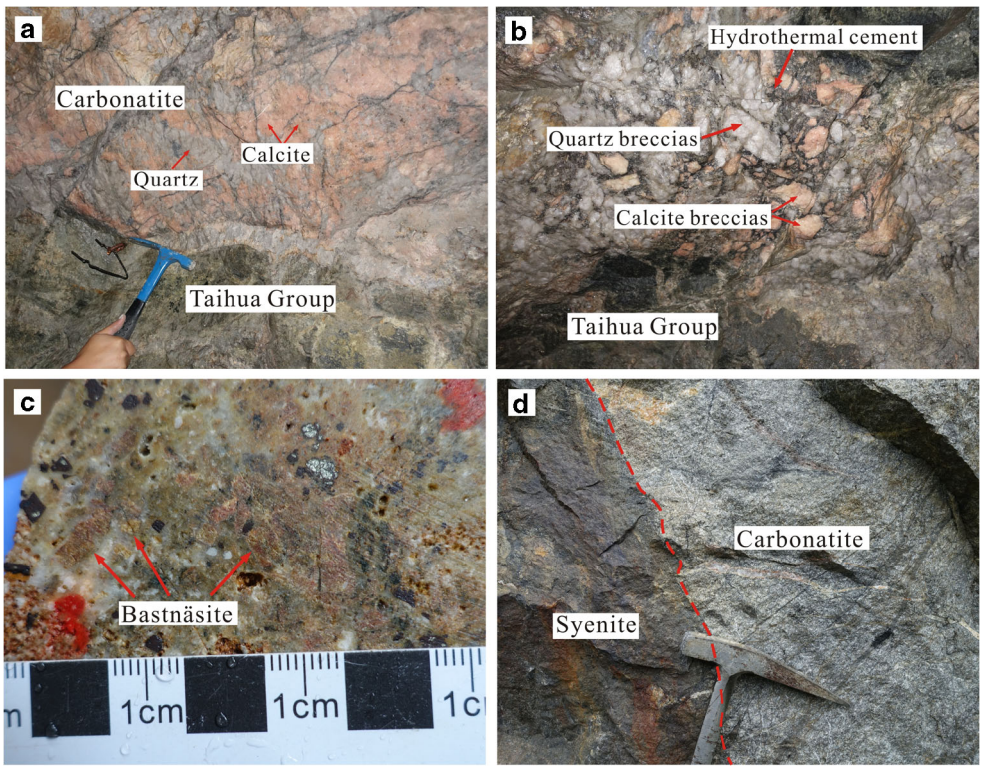

Fig. 2 Photographs of various ores from different REE deposits in the Qinling Orogenic Belt. **a** Carbonatite crosscut by hydrothermal veins in the Huangshuian deposit. Note that the pink mineral is calcite. **b** Breccia-type ore in the Huangshuian deposit, which consists of carbonatite (calcite) and quartz clasts cemented by REE-bearing hydrothermal matrix; **c** high-grade REE ores in the Taipingzhen deposit. Note that the greenish and pink crystals are bastnäsite grains. **d** Carbonatite dikes in the syenite of the Miaoya deposit

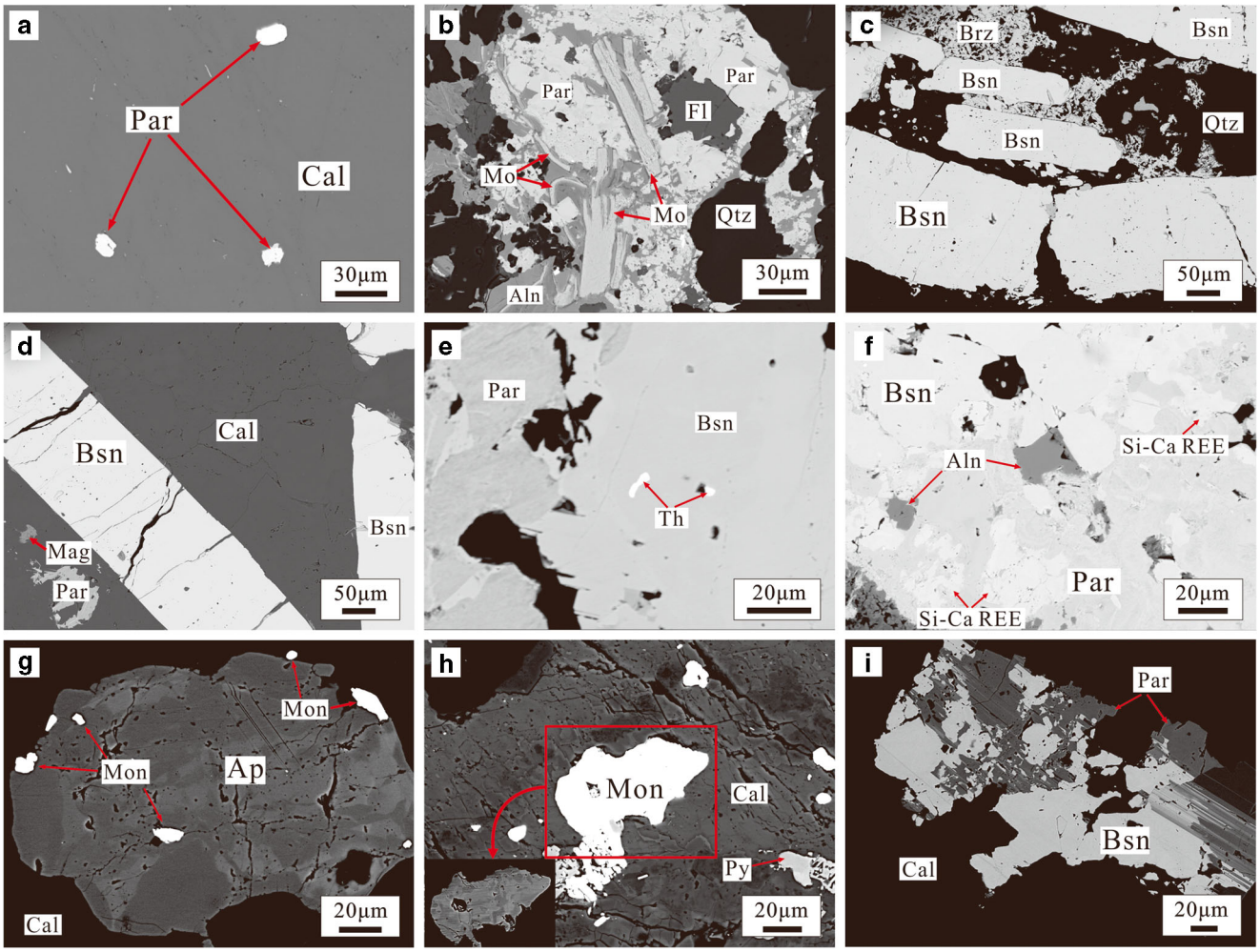

Fig. 3 BSE images of various REE ores in different deposits. **a** Disseminated parisite grains in carbonatite of the Huangshuian deposit. **b** Intergrowth of molybdenite and REE minerals (parisite and allanite) in the Huangshuian deposit. **c** Euhedral bastnäsite grains in REE ores of the Taipingzhen deposit. **d** REE-rich carbonatite of the Taipingzhen deposit, which is composed mainly of bastnäsite, parisite and calcite. **e** Intergrowth of bastnäsite and parisite in the ores of Taipingzhen deposit. **f** Intergrowth of bastnäsite, parisite, allanite, and unidentified Si-Ca REE minerals in the Taipingzhen deposit. **g** Fluorapatite with complex internal texture in the Miaoya deposit. Note that monazite inclusions are only present in the dark domains. **h** Anhedral monazite crystals in the carbonatite of the Miaoya deposit, note that the figure in the left bottom is the high-contrast BSE image of the monazite showing complex internal texture. **i** Intergrowth of bastnäsite and parisite in the Miaoya deposit. Abbreviations: Cal: calcite, Par: parisite, Bsn: bastnäsite, Qtz: quartz, Mo: molybdenite, Fl: fluorite, Aln: allanite, Th: thorite, Si-Ca REE: the unidentified Si-Ca REE minerals, Mag: magnetite, Brz: barite, Ap: apatite, Mnz: monazite, Py: pyrite

There are also minor synchysite and unidentified LREE silicates which are locally present as intergrowth with bastnäsite and parisite (Fig. 3f). The carbonatites consist mainly of calcite (~ 80%) and a small amount of quartz, biotite, pyrite, magnetite, and REE minerals. It is important to note that some carbonatites contain up to 10 vol% of REE minerals, and the REE minerals are dominated by bastnäsite with minor parisite and monazite (Fig. 3d).

Miaoya REE-Nb deposit

The Miaoya REE-Nb deposit is located in the southern margin of the Wudang Terrane of the South Qinling unit (Fig. 1b). The deposit contains more than 40 REE-Nb ore bodies with an estimated reserve of 1.21 Mt. REE_2O_3 @ 1.5 wt.% and 0.93 Mt. Nb_2O_5 @ 0.1 wt.% (Qian and Li 1996), making it the largest REE deposit in the Qinling Orogenic Belt. Ore bodies are hosted in the Miaoya syenite-carbonatite complex which covers an area of 6.5 km^2 and intrudes both the Neoproterozoic meta-quartz keratophyre of the Yaolinghe Group and Silurian schist of the Meiziya Group (Fig. 1e). Syenite dominates the Miaoya complex and has a zoned structure ranging from fine-grained in the center, allotriomorphic granular in the middle, to porphyritic in the margins. However, the syenites in different zones are mineralogically similar, and are composed dominantly of K-feldspar and subordinate microcline, albite, biotite, plagioclase, quartz, and

sericite with minor but variable amounts of zircon, monazite, columbite, fluorapatite, bastnäsite, pyrochlore, Nb-rich rutile, and pyrite. On the other hand, carbonatites in the Miaoya complex are present as stocks and/or dikes distributed in the syenites (Fig. 2d). They are dominated by medium- to fine-grained calcite (80%) with variable K-feldspar, albite, biotite, fluorapatite, monazite, columbite, bastnäsite, ilmenite, pyrochlore, aeschynite, quartz, Nb-rich rutile, and sulfides.

The REE ores are essentially REE-Nb-mineralized (economic) syenites and carbonatites in the complex. The major REE or REE-bearing minerals in the Miaoya deposit are fluorapatite, monazite, bastnäsite, and parisite (Fig. 3g–i). The fluorapatite grains are generally euhedral to subhedral, distributing in the interstitial matrix of K-feldspar and calcite in the syenite and carbonatite. They commonly exhibit complex internal textures that are characterized by bright and dark domains under BSE images, and the dark domains commonly contain fine-grained monazite inclusions (1–15 μm) (Fig. 3g). In addition to the monazite inclusions, most of monazite grains are present as anhedral grains in interstitial matrix replacing or crosscutting K-feldspar and calcite. These monazite grains have relatively large but variable sizes (10–200 μm) and commonly appear inhomogeneous under BSE (Fig. 3h), even though several appear homogeneous. Bastnäsite is locally present, occurring as subhedral crystals replacing major minerals or as single grains in veinlets containing quartz, calcite, barite, and fluorite (Fig. 3i). In veinlets, the bastnäsite grains are generally embayed and crosscut by calcite, K-feldspar, quartz, and minor fluorite. Other REE minerals include allanite, synchysite, and ancylite, but they are sporadically distributed and commonly intergrown with the major REE minerals mentioned above.

Analytical method

Representative REE ore samples for dating were collected from the Huangshuian, Taipingzhen, and Miaoya deposits. These samples were polished as thin sections, and textural relationships examined using a standard optical microscope, followed by JSM-7800F field emission scanning electron microscopy (FE-SEM) equipped with TEAM Apollo XL energy disperse spectroscope at the State Key Laboratory of Ore Deposit Geochemistry, Institute of Geochemistry, Chinese Academy of Sciences.

U-Th-Pb isotopic analyses of bastnäsite and monazite in polished thin section were carried out using ICP-MS (Agilent 7700×) with a Laser-ablation system (ASI RESOnetics S-155, 193 wavelength) at Nanjing FocuMS Technology Co. Ltd. Detailed analytical procedures and instrumental operating conditions are available in Yang et al. (2014). Analyses were performed with a beam diameter of 24 μm and a repetition rate of 6 Hz. At the start of each analytical session, torch position and lens tunings were adjusted to maximize sensitivity for the appropriate masses (Pb isotopes, Th and U) and stability. The initial conditions were set at $ThO^+/Th^+ < 0.3\%$ to minimize the production of molecular compounds. Each spot analysis consisted of an approximate 20-s background acquisition and 65-s sample data acquisition. The U-Th-Pb fractionation and instrumental mass discrimination of bastnäsite were normalized using the matrix-matched external bastnäsite standard K-9 (118 ± 1 Ma; Sal'nikova et al. 2010). For the monazite, the analysis results were normalized to the known value standard 44,069 (424 ± 1 Ma; Aleinikoff et al. 2006). Two standard analyses were measured after every five unknown bastnäsite or monazite spots. Off-line data selection and integration were performed by using ICPMSDataCal software (Liu et al. 2010), and age calculations were processed using the ISOPLOT program (Ludwig 2003). Uncertainties associated with age determinations are 1 sigma and ages were calculated at the 95% confidence level.

U-Th-Pb ages of bastnäsite and monazite

Due to the relatively small sizes of the monazite, only bastnäsite in the Huangshuian and Taipingzhen deposits are analyzed for U-Th-Pb dating, whereas both bastnäsite and monazite in the Miaoya deposits were available for U-Th-Pb dating. The U-Th-Pb isotopic results of the bastnäsite and monazite are shown in Appendices 1 and 2, respectively.

Huangshuian deposit

Bastnäsite grains analyzed are homogeneous under BSE image. They have U and Th contents ranging from 25 to 506 ppm and 4051 to 16,338 ppm (Appendix 1), respectively, corresponding to high Th/U ratios (138 in average). On the Tera-Wasserburg plot (Tera and Wasserburg 1972a, 1972b), 20 analyses of uncorrected data give a lower intercept age of 223.0 ± 7.2 Ma (MSWD = 4.6; Fig. 4a). Excluding several spots that have obviously lower or higher $^{206}Pb/^{238}U$ ages, a weighted average $^{206}Pb/^{238}U$ age of 215.6 ± 3.8 Ma ($n = 17$; MSWD = 1.9; Fig. 4b) is obtained after ^{207}Pb-based correction method, which using common Pb composition from Stacey and Kramers (1975) (Appendix 1). After correction for common Pb (Appendix 1), the weighted average $^{208}Pb/^{232}Th$ age is calculated to be 201.2 ± 1.6 Ma ($n = 18$; MSWD = 1.8; Fig. 4c).

Taipingzhen deposit

The bastnäsite grains in the REE ores from the Taipingzhen deposit have U and Th concentrations ranging from 26 to

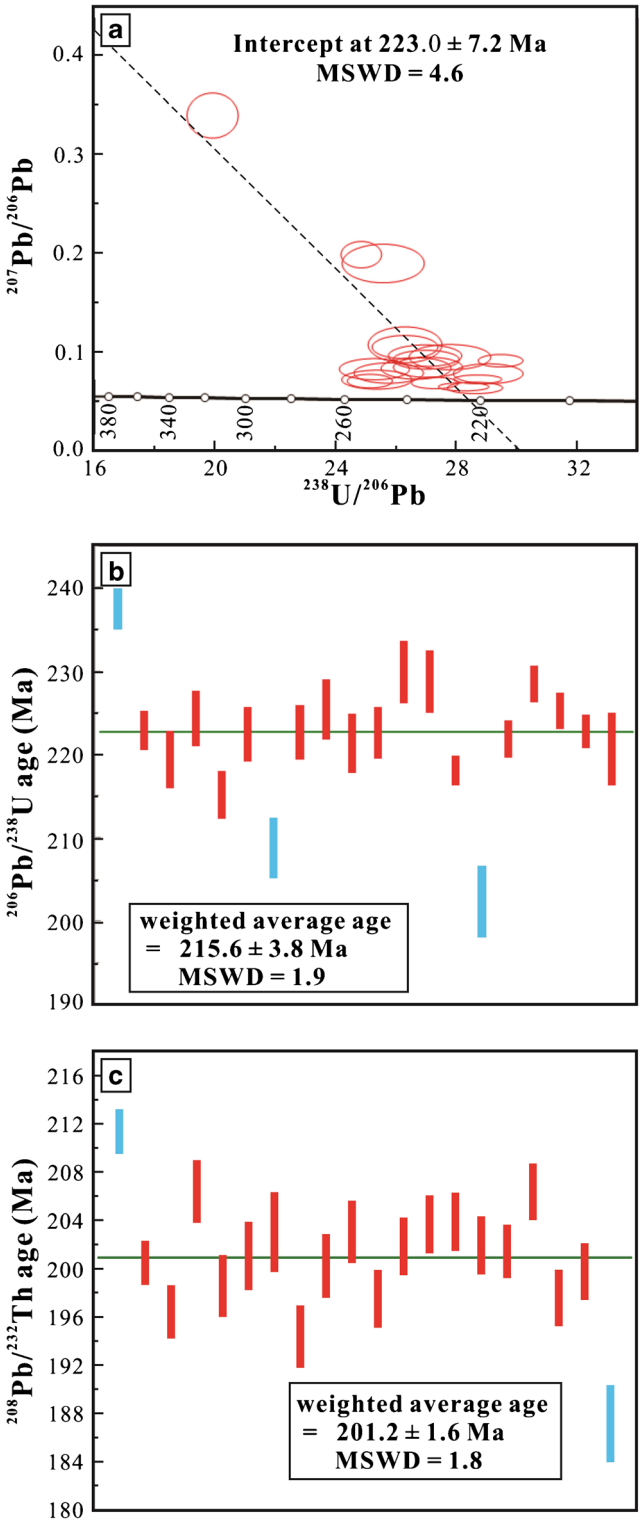

Fig. 4 LA-ICP-MS U-Th-Pb ages of the bastnäsite from the Huangshuian deposit. **a** Tera-Wasserburg plots of U-Pb ages. **b** Weighted average ^{206}Pb/^{238}U ages (^{207}Pb-based corrected). **c** Weighted average ^{208}Pb/^{232}Th ages (common Pb-corrected)

101 ppm and 4014 to 13,936 ppm, respectively, corresponding to high Th/U ratios ranging from 95 to 435. On the Tera-Wasserburg plot, 20 analyses define a regression line yielding a lower intercept age of 424 ± 22 Ma (MSWD = 2.6; Fig. 5a). After ^{207}Pb-based correction, a weighted average ^{206}Pb/^{238}U age of 420.7 ± 7.3 Ma (n = 16; MSWD = 1.5) is obtained (Fig. 5b), slightly older than the weighted average ^{208}Pb/^{232}Th age of 411.8 ± 5.5 Ma (common Pb-corrected; n = 17; MSWD = 4.5; Fig. 5c).

Bastnäsite grains in carbonatites have Th and U content and Th/U ratios comparable with those in the hydrothermal ores (Appendix 1). Twenty-four analyses yield a lower intercept age of 435.0 ± 4.8 Ma (n = 24; MSWD = 1.4) on the Tera-Wasserburg plot (Fig. 5d). After ^{207}Pb-based correction, a weighted average ^{206}Pb/^{238}U age of 430.4 ± 4.8 Ma (n = 24; MSWD = 1.4) is calculated (Fig. 5e), slightly older than the weighted average ^{208}Pb/^{232}Th age of 411.9 ± 3.8 Ma (common Pb-corrected; n = 23; MSWD = 2.6; Fig. 5f).

Miaoya deposit

Bastnäsite grains have U and Th concentrations ranging from 7 to 173 ppm and 2284 to 8778 ppm, respectively, corresponding to Th/U ratios varying from 44 to 501. Eighteen analyses form a well-fitting regression line defining a lower intercept age of 209.8 ± 9.8 Ma (MSWD = 1.9) on the Tera-Wasserburg plot (Fig. 6a). After ^{207}Pb-based correction, a weighted average ^{206}Pb/^{238}U age of 205.8 ± 3.6 Ma is also obtained (n = 14; MSWD = 1.5; Fig. 6b). The weighted average ^{208}Pb/^{232}Th age is 206.5 ± 2.8 Ma (common Pb-corrected; n = 14; MSWD = 3.6; Fig. 6c).

Both the BSE-homogenous and inhomogeneous monazite grains were selected for dating. These monazite grains have higher U and lower Th content than the bastnäsite grains, with a lower Th/U ratio of 41 in average (Appendix 2). On the Wether ill concordia plot (Wetherill 1956), a total of 50 analyses yield highly scattered plots but forming two groups of ages that are well correlated with the internal textures and compositions (Fig. 7a). The first group of analyses, obtained from the BSE-inhomogeneous grains, has a wide U-Pb age range (Fig. 7a) but a portion of them clusters on the concordant line with a calculated weighted average ^{206}Pb/^{238}U age of 231.0 ± 2.3 Ma (n = 21; MSWD = 3.1; Fig. 7b), undistinguishable from those obtained by the same method in previous studies (e.g., Xu et al. 2014; Ying et al. 2017). Another group of analyses, obtained from the homogeneous grains, have only five U-Pb age data because only a few grains were recovered from the deposit. However, these analyses have a consistent ^{206}Pb/^{238}U age with weighted average of 414 ± 11 Ma (MSWD = 0.91; Fig. 7c), close to the zircon U-Pb age of the Miaoya carbonatite at 434.3 ± 3.2 Ma and 426.5 ± 8.0 Ma previously dated by Zhu et al. (2016) and Ying et al. (2017), respectively. The ages that deviated from the concordant line are mostly obtained from domains of complex BSE

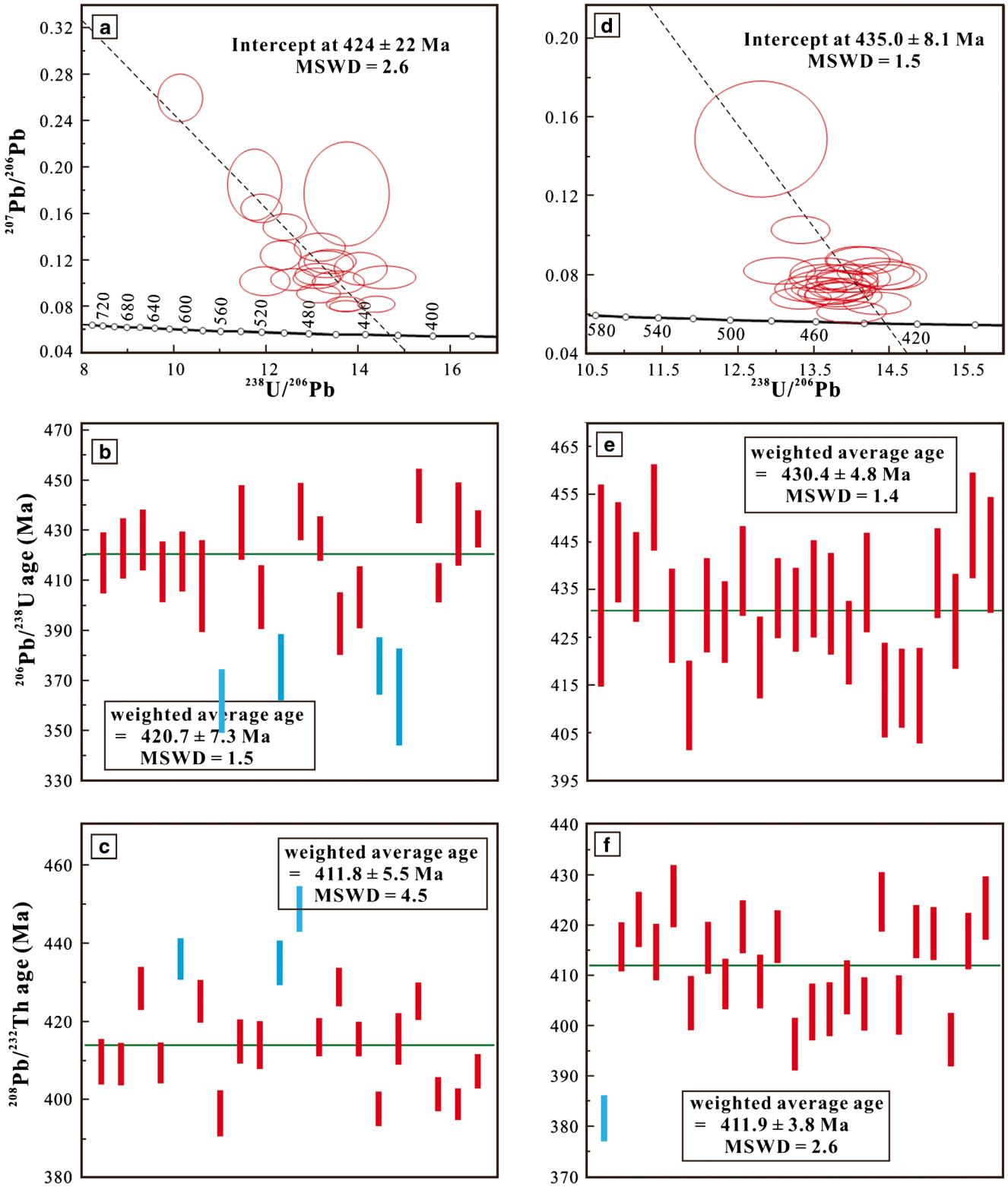

Fig. 5 LA-ICP-MS U-Th-Pb ages of the bastnäsite from the REE ores and REE-rich carbonatites in the Taipingzhen deposit. **a** Tera-Wasserburg plots U-Pb ages, **b** weighted average $^{206}Pb/^{238}U$ (^{207}Pb-based corrected), and **c** $^{208}Pb/^{232}Th$ (common Pb-corrected) ages of bastnäsite from the REE ores. **d** Tera-Wasserburg plots U-Pb ages, **e** weighted average $^{206}Pb/^{238}U$ (^{207}Pb-based corrected), and **f** $^{208}Pb/^{232}Th$ (common Pb-corrected) ages of bastnäsite from the REE-rich carbonatites

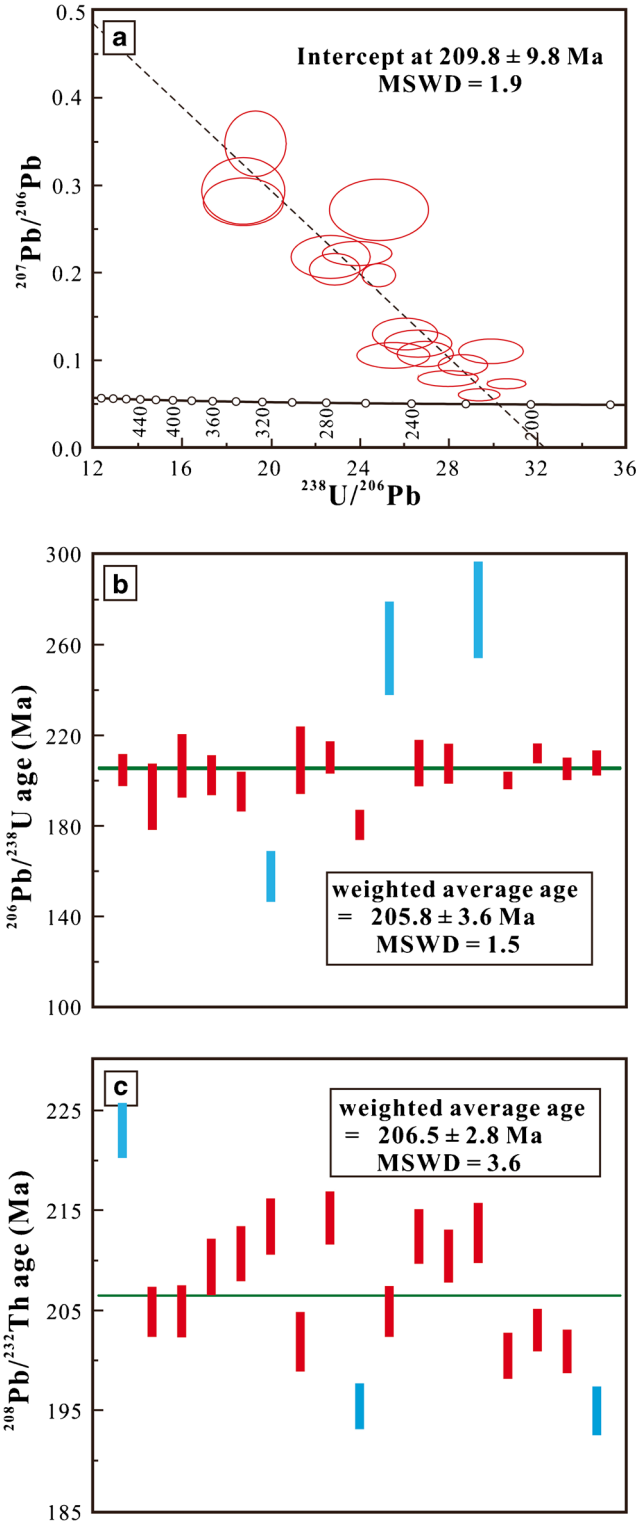

Fig. 6 LA-ICP-MS U-Th-Pb ages of bastnäsite in veinlets from the Miaoya deposit. **a** Tera-Wasserburg plots of U-Pb ages. **b** Weighted average $^{206}Pb/^{238}U$ ages (^{207}Pb-based corrected). **c** Weighted average $^{208}Pb/^{232}Th$ ages (common Pb-corrected)

images (Fig. 7d), possibly representing mixing ages, which resulted from incomplete alteration or replacement.

Discussion

Reliability of the U-Th-Pb ages of the bastnäsite and monazite

Bastnäsite and monazite have long been widely and successfully used for U-Th-Pb dating (e.g., Parrish 1990; Yang et al. 2014; Ling et al. 2016). However, both bastnäsite and monazite are commonly Th-rich minerals with extremely high Th/U ratios (e.g., up to 1000; Parrish 1990; Ling et al. 2016), thus containing considerable amounts of excess ^{206}Pb derived from initially incorporated ^{230}Th and resulting in overestimation of the $^{206}Pb/^{238}U$ ages. In this study, some of the bastnäsite grains from the Huangshuian, Taipingzhen, and Miaoya deposits do have high Th contents (up to 20,000 ppm; Appendix 1) with Th/U ratios up to 500, and their $^{208}Pb/^{232}Th$ ages are mostly younger than the $^{206}Pb/^{238}U$ ages (Figs. 4, 5, and 6), indicative of potential effect of excessed ^{206}Pb. In general, such an effect can be avoided by correcting the $^{206}Pb/^{238}U$ ages for excessed ^{206}Pb using the equations of Schärer (1984) and Parrish (1990) (Table 1), or by using only the $^{208}Pb/^{232}Th$ ages (e.g., Gregory et al. 2007; Ling et al. 2016). However, it is generally considered that Th is easily incorporated into or taken away from Th-rich minerals during alteration (Rasmussen and Muhling 2007; Harlov et al. 2011), and the $^{208}Pb/^{232}Th$ age was indicated by experiments to be more sensitive to the variation of Th than $^{206}Pb/^{238}U$ age (Poitrasson et al. 2000). Therefore, it is possible that the ^{232}Th-^{208}Pb radiometric system was relatively easier to be disturbed during later hydrothermal alteration. Indeed, such an interpretation is supported by the high MSWDs of the $^{208}Pb/^{232}Th$ ages or scatter of the $^{208}Pb/^{232}Th$ ratios in this study (Figs. 4, 5, and 6). As such, following the equation of Schärer (1984) and Parrish (1990), we re-calculated $^{206}Pb/^{238}U$ ages of these samples on the basis of the estimated Th/U ratios of the parental fluids/melts (Table 1). These corrected $^{206}Pb/^{238}U$ ages were then compared U ratios upe $^{208}Pb/^{232}Th$ ages to understand the reliability of the new U-Th-Pb ages.

The calculated results show that the excessed ^{206}Pb-corrected $^{206}Pb/^{238}U$ ages are indeed variably younger (< 1, 4.6, and 9.1 Ma) than those uncorrected (Table 1). Although these corrected ages are slightly different from $^{208}Pb/^{232}Th$ ages (Figs. 4, 5, and 6; Table 1), the fact that the corrected $^{206}Pb/^{238}U$ age (207 Ma) of the Huangshuian deposit (Table 1) is identical to the molybdenite Re-Os ages (~ 208 Ma; Huang et al. 2009; Cao et al. 2014) suggests that the corrected $^{206}Pb/^{238}U$ ages are more reliable, which in turn suggests that the $^{208}Pb/^{232}Th$ ages are more or less disturbed, as indicated earlier. It is notable that the bastnäsite $^{206}Pb/^{238}U$ ages of both the ores in the Taipingzhen deposit and the veinlets of the Miaoya deposit were not corrected for excess ^{206}Pb because the Th/U ratios of their parental fluids cannot be estimated (Table 1). However, in the case of the Taipingzhen deposit,

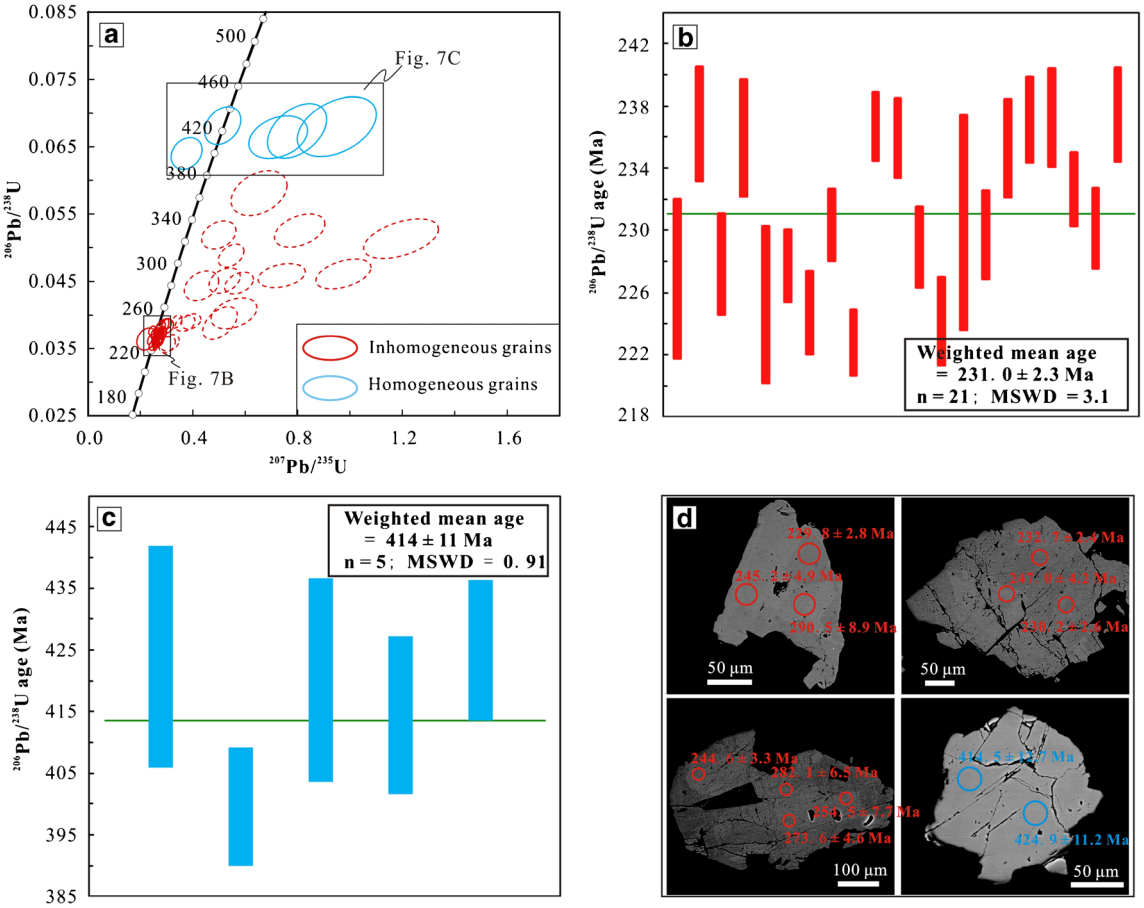

Fig. 7 LA-ICP-MS U-Th-Pb ages of the monazite from the Miaoya deposit. **a** Concordia plot of LA-ICP-MS U-Pb data for both BSE-inhomogeneous (red circles) and BSE-homogeneous (blue circles) monazite grains. **b** Weighted average $^{206}Pb/^{238}U$ age of the BSE-inhomogeneous grains, which is calculated by 21 analyses clustering on the concordant line. **c** Weighted average $^{206}Pb/^{238}U$ age of the BSE-homogeneous grains. **d** BSE images of several grains that show location of analyzed spots and corresponding ages. Note that the top two and bottom left one are BSE-inhomogeneous grains whereas the bottom right one is BSE-homogeneous grain with obviously older ages

the effect of excessed ^{206}Pb should be negligible due to extremely high Th/U ratios of the fluids as suggested by the presence of thorite in the ores (Fig. 3e), if calculated by using the equation of Schärer (1984) and Parrish (1990). Similarly, in the case of the veinlets of the Miaoya deposit, the effect of excessed ^{206}Pb is also speculated to be negligible on the basis of the fact that the uncorrected $^{206}Pb/^{238}U$ age is indistinguishable from the $^{208}Pb/^{232}Th$ age (Fig. 6).

Table 1 Correction of excess ^{206}Pb derived from initially incorporated ^{230}Th for the $^{206}Pb/^{238}U$ ages

Deposit	Th/U (whole rock)	Th/U (mineral)	f	T_{excess} (Ma)	$^{206}Pb/^{238}U$ age (excess ^{206}Pb corrected)
Huangshuian	1.62 (carbonatite)	138 (Bsn)	85.19	9.1	206.5
Taipingzhen	Unknown (ores)	249 (Bsn)	/	/	/
	5.23 (carbonatite)	225 (Bsn)	43.02	4.6	425.6
Miaoya	Unknown (veinlet)	218 (Bsn)	/	/	/
	5.4 (carbonatite)	41 (Mnz)	7.59	< 1	Uncorrected

$T_{excess} = (1/\lambda_{238})$ In $[1 + (f - 1)(\lambda_{238}/\lambda_{230})]$ (Schärer 1984; Parrish 1990)

$f = [(Th/U)_{mineral}/(Th/U)_{liquid}]$; $\lambda_{238} = 1.55125e^{-10}$ year^{-1}; $\lambda_{230} = 0.922e^{-5}$ year^{-1}

The value of (Th/U) liquid was calculated from whole-rock Th and U concentrations assuming magma (liquid) was in radioactive equilibrium before mineral crystallization (Parrish 1990)

Note that the whole rock Th/U ratios of carbonatites in the Huangshuian and Taipingzhen deposits is from our unpublished data, and that of the Miaoya deposit is cited from Xu et al. (2014)

Abbreviations: *Bsn* bastnäsite; *Mnz* monazite

In summary, it is believed that after corrections of the common Pb and excessed ^{206}Pb, the $^{206}Pb/^{238}U$ ages are more reliable to represent the timing of the REE mineralization in the Qinling Orgogenic Belt. It is thus concluded that the REE mineralization of the Huangshuian and Taipingzhen deposits has formed at 207 Ma and 426–421 Ma, respectively, whereas the REE minerals in the Miaoya deposit have formed at two stages of 414 Ma and 231–206 Ma.

Two episodes of REE mineralization

The new U-Th-Pb dating results of bastnäsite and monazite provide comprehensive constraints on the timing of the REE mineralization in the Qinling Orogenic Belt. In the North Qinling unit, we provide a reliable REE mineralization age of 426–421 Ma for the newly discovered Taipingzhen deposit. In the Southern North China Craton, the timing of the REE mineralization in the Huangshuian deposit is constrained to be ~ 207 Ma, indicating a much younger mineralization event. These ages are also broadly similar to the molybdenite Re-Os and monazite U-Th-Pb ages (220–210 Ma) of the Huanglongpu Mo-(REE) deposit in the same unit (Table 2), thus allowing us to propose that the carbonatite-related Mo and REE mineralization in the Southern North China Craton of the Qinling Orogenic Belt was formed at 220–200 Ma.

For the Miaoya deposit in the South Qinling unit, ages of ~ 415 Ma and 231–206 Ma were both obtained from the REE minerals. The older ages are broadly similar to the zircon LA-ICP-MS U-Pb ages of 445–426 Ma for the Miaoya and nearby Shaxiongdong syenite-carbonatite complexes (Xu et al. 2008; Lu et al. 2014; Zhu et al. 2016; Ying et al. 2017), thus indicating an early REE mineralization event possibly genetically related to the formation of the syenite-carbonatite complex. On the other hand, the younger ages of 231–206 Ma, which were also reported in other studies (e.g., Xu et al. 2014; Ying et al. 2017), were once suggested to represent a younger, new REE mineralization event in the region (Xu et al. 2014; Cimen et al. 2018). However, considering the fact that these ages are obtained on the monazite with complex internal textures or on the bastnäsite from veinlets crosscutting the REE-mineralized carbonatites and syenites, we propose that they more likely record a secondary REE remobilization or hydrothermal overprint event that locally modified the early REE minerals. Similar internal textures that are indicative of secondary hydrothermal

Table 2 Summary of geochronological data for the REE deposits in the Qinling Orogenic Belt

Tectonic unit	Deposit	Sample type	Method	Age (Ma)	Reference
S-NCC	Huangshuian	Carbonatites	Molybdenite Re-Os (ICP-MS)	209.5 ± 4.2	Huang et al. 2009
		Carbonatites	Molybdenite Re-Os (ICP-MS)	208.4 ± 3.6	Cao et al. 2014
		Breccia	Molybdenite Re-Os (ICP-MS)	217.1 ± 8.5	Lu et al. 2014
		Carbonatites	BastnäsiteTh-Pb (LA-ICP-MS)	206.5 ± 3.8	This study
	Huanglongpu	Carbonatites	Molybdenite Re-Os (ICP-MS)	221.5 ± 0.3	Stein 1997
		Carbonatites	Molybdenite Re-Os (ICP-MS)	222 ± 7	Huang et al., 1995
		Carbonatites	Molybdenite Re-Os (ICP-MS)	225 ± 7.6	Song et al. 2015
		Carbonatites	Monazite U-Th-Pb (LA-ICP-MS)	208.9 ± 4.6 and 213.6 ± 4.0	Song et al. 2016
NQL	Taipingzhen	Ores	BastnäsiteTh-Pb (LA-ICP-MS)	420.7 ± 7.3	This study
		Carbonatites	BastnäsiteTh-Pb (LA-ICP-MS)	425.6 ± 4.8	This study
SQL	Shaxiongdong	Syenite	Zircon U-Pb (LA-ICP-MS)	441.8 ± 2.2	Xu et al. 2008
		Carbonatites	Apatite Th-Pb (LA-ICP-MS)	433.1 ± 6.4	Lu et al. 2014
	Miaoya	Carbonatites	Monazite U–Th–Pb (SHRIMP)	233.6 ± 1.7	Xu et al. 2014
		Syenite	Zircon U-Pb (LA-ICP-MS)	445.2 ± 2.6	Zhu et al. 2016
		Carbonatites	Zircon U-Pb (LA-ICP-MS)	434.3 ± 3.2	Zhu et al. 2016
		Carbonatites	Zircon U-Th-Pb (LA-ICP-MS)	426.5 ± 8.0	Ying et al. 2017
		Syenite	Zircon U-Th-Pb (LA-ICP-MS)	442.6 ± 3.7	Ying et al. 2017
		Carbonatites	Columbite U-Pb (LA-ICP-MS)	232.8 ± 3.7	Ying et al. 2017
		Syenite	Monazite Th-Pb (LA-ICP-MS)	243.1 ± 2.5	Ying et al. 2017
		Carbonatites	Monazite Th-Pb (LA-ICP-MS)	238.3 ± 4.1	Ying et al. 2017
		Carbonatites	Bastnäsite U-Th-Pb (LA-ICP-MS)	205.8 ± 3.6	This study
		Carbonatites	Monazite U-Pb (LA-ICP-MS)	414 ± 11	This study
		Carbonatites	Monazite U-Pb (LA-ICP-MS)	231.0 ± 2.3	This study

modifications are also available in apatite. For example, fluorapatite grains are commonly characterized by bright and dark domains under BSE images, and the dark domains contain inclusions of monazite (Fig. 3g). This texture was well interpreted to be formed by a dissolution-reprecipitation process that is related to the apatite-fluid interaction (e.g., Harlov and Förster 2003; Harlov et al. 2005; Chen and Zhou 2015). Such a process is able to partially or fully reset the U-Th-Pb isotopic system (Williams et al. 2011; Chen and Zhou 2017; Grand'Homme et al. 2017), and is thus likely responsible for the discordant analyses with variable $^{206}Pb/^{238}U$ ages of monazite (e.g., the plots marked by red dash circles in Fig. 7a).

In summary, our precise constraints on the timing of the REE mineralization in different units of the Qinling Orogenic Belt reveal two episodes of REE mineralization at 440–410 and 220–200 Ma (Fig. 8). The first episode is present in the North Qinling and South Qinling units and some deposits of this episode suffered from secondary hydrothermal overprint, such as the Miaoya deposit. The second episode is present in the Southern North China Craton and is closely associated with Mo mineralization, such as the Huanglongpu and Huangshuian deposits.

Implication for tectonic setting and regional metallogeny

The Qinling Orogenic Belt is a composite orogenic belt involving multi-stage processes of arc terrane accretion, arc-continent, and continent-continent collisions between the North and South China Cratons. The North Qinling unit was separated from the South China Craton at ca. 0.80 Ga during the Rodinian breakup, followed by accretion northward to the North China Craton (Ratschbacher et al. 2003; Wu and Zheng 2013). The northward subduction of the North Qinling resulted in the formation of the Erlangping arc, which was developed to be a back-arc basin after the collision between the North Qinling unit and North China Craton at Silurian. At the same time, the South Qinling unit was also separated from the South China Craton as a consequence of the opening of the Mianlue Ocean (Meng and Zhang 1999, 2000). Northward subduction of the Mianlue oceanic crust resulted in the amalgamation of the South Qinling and North Qinling units at Carboniferous and the final collision of North China Craton and South China Craton at Triassic (Dong and Santosh 2016; Li et al. 2007; Wu and Zheng 2013).

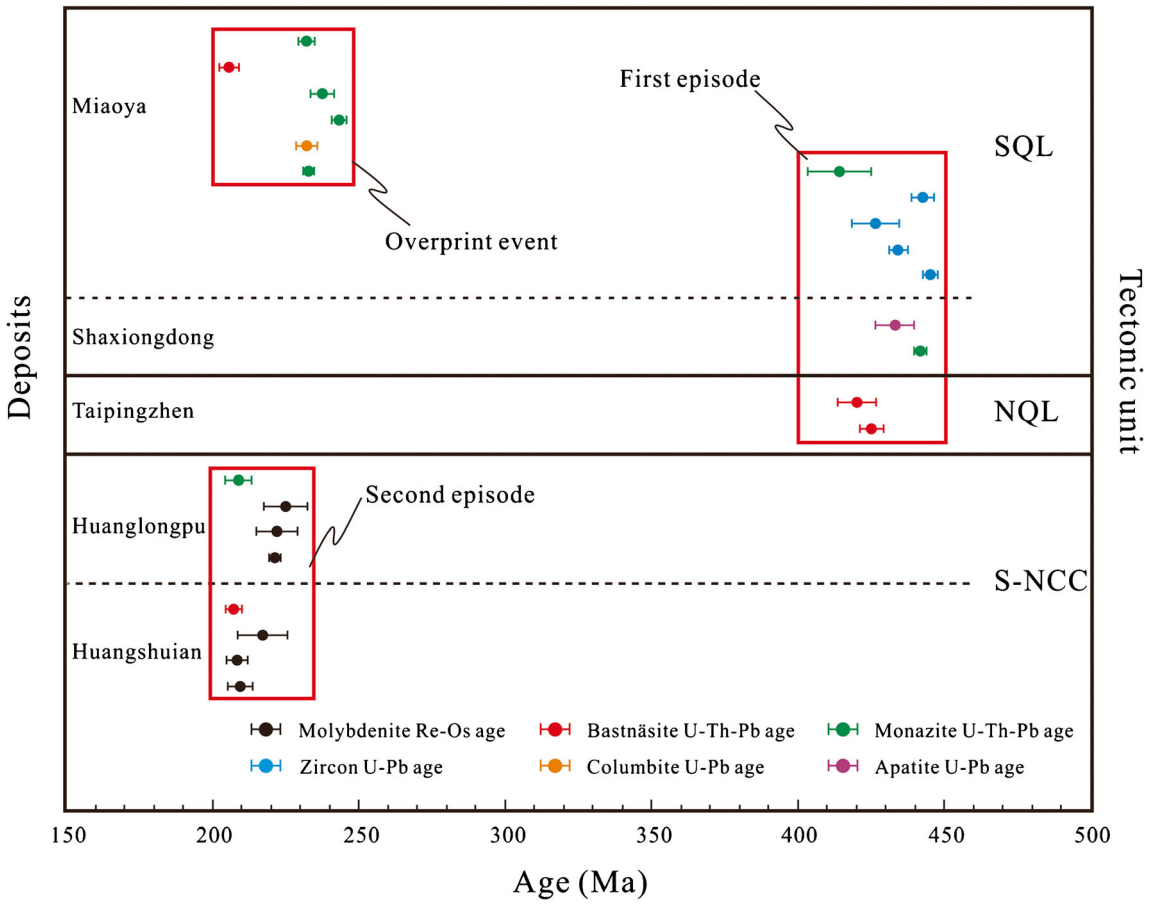

Fig. 8 Summary of geochronological data for the REE deposits in the Qinling Orogenic Belt. The data and references are available in Table 2

Precise dating of the REE mineralization in the Qinling Orogenic Belt thus provides important implications for tectonic environment of the mineralization which is correlated well with the tectonic evolution of the orogenic belt as described above. The early, 440–410 Ma episode of REE mineralization is present in both the North Qinling and South Qinling units. Such an episode of REE mineralization in the North Qinling is synchronous with back-arc magmatism, such as the Kanfengkou granodiorite (440 Ma; Abdallsamed et al. 2017) and Taoyuan granite (429 Ma; Zhang et al. 2001b), and thus was interpreted to be formed in an extension setting related to the opening of Erlangping back-arc basin at Silurian. In the South Qinling, this episode of REE mineralization is synchronous with rifting-related magmatic rocks in the region, such as the Huangyangshan granite (439 ± 6 Ma; Ma et al. 2005) and Lianghekou gabbroic dikes (421 ± 4.7 Ma; Chen et al. 2014), indicating that it has formed in a rifting setting that is likely related to the opening of Mianlue Ocean at Silurian.

It was considered that the final collision between the North and South China Cratons occurred at the Middle Triassic (230–220 Ma) along the Mianlue suture at the south edge of South Qinling unit (Meng and Zhang 1999; Dong and Santosh 2016). This collision resulted in widespread magmatic-hydrothermal activities in the South Qinling unit (Chen and Santosh 2014; Qin et al. 2007; Gong et al. 2009) and thus is likely responsible for the late overprint event of 231–206 Ma in the Miaoya deposit. On the other hand, the late, 220–200 Ma episode of REE mineralization that is present in the Southern North China Craton is coeval with widespread alkaline rocks in the region, such as the Mogou aegirine-augite syenite (210–237 Ma; Cao et al. 2015), Dongjikou pyroxene syenite (213–215 Ma; Li et al. 2012a), and Zhaiwa syenogranite (217 Ma; Li et al. 2012b). These alkaline rocks were interpreted to reflect a post-collisional extension event locally present in the Southern North China Craton (Cao et al. 2015; Li et al. 2012a), thus indirectly indicating that the Triassic episode of REE mineralization in this region has formed in an extensional setting.

Our new results also have important implications for regional REE exploration in the Qinling Orogenic Belt. Further exploration in the currently discovered Taipingzhen deposit in the Northern Qinling unit has revealed REE-rich pegmatite rocks around the Taipingzhen deposit (Henan Nuclear Geological Bureau, unpublished internal report, 2018). Similar 430–410 Ma REE-rich pegmatites were also reported in other locations of the unit (Wan et al. 1992; Feng 1996; Zhu et al. 2015; Yuan et al. 2017, 2018; Wang et al. 2018). Although these pegmatites are currently targets for only uranium and rare metal mining, our new dating results of the Taipingzhen deposit indicate that the regions where these pegmatites are present can be also potential candidates for REE exploration. In the South Qinling unit, current exploration revealed only the 440–410 Ma Miaoya and Shaxiongdong REE-Nb deposits. However, REE-enriched alkaline rocks of the same ages are potentially widespread in the unit, including the Tianbao trachyte (430 Ma; Wan et al. 2016), Haoping quartz syenite and Guanzishan nepheline syenite (435–440 Ma; Wang et al. 2017) and Langao alkali lamprophyre complex (432 Ma; Xu et al. 2013). Although these alkaline rocks are currently not a target for REE mining, exploration activities have already revealed that some of these alkaline rocks are locally REE-mineralized (Wu et al. 2015; Zhu et al. 2017). We believe that further explorations focusing on the 440–410 Ma alkaline rocks in the South Qinling unit will reveal more potential candidates for REE mining.

Conclusions

In situ U-Th-Pb isotopic dating on the bastnäsite and monazite from several deposits in different units of the Qinling Orogenic Belt has revealed two episodes of REE mineralization at 440–410 and 220–200 Ma. The early episode is distributed in the North Qinling and South Qinling units, corresponding to the opening of Erlangping back-arc basin and Mianlue Ocean, respectively. The second episode is mainly present in the Southern North China Craton and was related to the locally extensional event after final collision of the Qinling Orogenic Belt at Triassic. This study also provides important implications that the 440–410 Ma pegmatite and alkaline rocks in the North Qinling and South Qinling units, respectively are potentially candidates for future REE exploration.

Acknowledgments We thank Prof. Xin-Chun Zhang from the Institute of Geochemistry, Chinese Academy of Sciences and Li-Min Chang, Wei-Dong Zhang, and Wen-Hui Yang from Henan Nuclear Geological Bureau for their valuable assistance during the field investigations. We also thank Liang Li and Rang-Tian Wu from Nanjing FocuMS Technology Co. Ltd. for the help during LA-ICP-MS analyses. We are grateful to the official reviews by Xin-Fu Zhao and Donald Davis, and editorial handling by Bernd Lehmann and Robert Linnen

Funding information This study is supported by the National Key R&D Program of China (2017YFC0602302) and Key Research Program of Frontier Sciences, CAS (QYZDB-SSW-DQC008).

References

Abdallsamed MIM, Wu YB, Zhang W, Zhou G, Hao W, Yang S (2017) Early Paleozoic high-Mg granodiorite from the Erlangping unit, North Qinling orogen, Central China: partial melting of metasomatic mantle during the initial back-arc opening. Lithos 288:282–294

Aleinikoff JN, Schenck WS, Plank MO, Srogi L, Fanning CM, Kamo SL, Bosbyshell H (2006) Deciphering igneous and metamorphic events in high-grade rocks of the Wilmington Complex, Delaware: morphology, cathodoluminescence and backscattered electron zoning, and SHRIMP U-Pb geochronology of zircon and monazite. Geol Soc Am Bull 118:39–64

Cao J, Ye H, Li H, Li Z, Zhang XK, He W, Li C (2014) Geological characteristics and molybdenite Re-Os isotopic dating of Huangshuian carbonatite vein-type Mo(Pb)deposit in Songxian County, Henan Province. Mineral Deposita 33:53–69 (in Chinese with English abstract)

Cao J, Ye HS, Li Z, Zhang XK, Wang P, He W (2015) Geochronology, geochemistry and petrogenesis of the Mogou alkalic pluton in the East Qinling orogenci belt. Acta Petrol Min 34:665–684 (in Chinese with English abstract)

Chen YJ, Santosh M (2014) Triassic tectonics and mineral systems in the Qinling Orogen, Central China. Geol J 49:338–358

Chen WT, Zhou MF (2015) Mineralogical and geochemical constraints on mobilization and mineralization of rare earth elements in the Lala Fe-Cu-(Mo, REE) deposit, SW China. Am J Sci 315:671–711

Chen WT, Zhou MF (2017) Hydrothermal alteration of magmatic zircon related to NaCl-rich brines: diffusion-reaction and dissolution-reprecipitation processes. Am J Sci 317:177–215

Chen H, Tian M, Wu GL, Hu JM (2014) The Early Paleozoic alkaline and mafic magmatic events in Southern Qinling Belt, Central China: evidences for the break-up of the Paleo-Tethyan Ocean. Geol Rev 60:1437–1452 (in Chinese with English abstract)

Cimen O, Kuebler C, Monaco B, Simonetti SS, Corcoran L, Chen W, Simonetti A (2018) Boron, carbon, oxygen and radiogenic isotope investigation of carbonatite from the Miaoya complex, Central China: evidences for late-stage REE hydrothermal event and mantle source heterogeneity. Lithos 322:225–237

Ding LX, Ma CQ, Li JW, Robinson PT, Deng XD, Zhang C, Xu WC (2011) Timing and genesis of the adakitic and shoshonitic intrusions in the Laoniushan complex, southern margin of the North China Craton: implications for post-collisional magmatism associated with the Qinling Orogen. Lithos 126:212–232

Dong Y, Santosh M (2016) Tectonic architecture and multiple orogeny of the Qinling Orogenic Belt, Central China. Gondwana Res 29:1–40

Feng M (1996) Discussion on the genesis of uranium-producing pegmatite in Shangdan area. Uranium Geol 12:30–36 (in Chinese with English abstract)

Gao C, Kang QQ, Jiang HJ, Zheng H, Peng LI, Zhang XM, Lei LI, Dong QQ, Ye XC, Hu XJ (2017) A unique uranium polymetallic deposit discovered in the Qinling orogenic belt: the Huayangchuan super-large U-Nb-Pb-REE deposit associated with pegmatites and carbonatites. Geochimica 46:446–455 (in Chinese with English abstract)

Gong HJ, Zhu LM, Sun BY, Li B, Guo B (2009) Zircon U–Pb ages and Hf isotope characteristics and their geological significance of the Shahewan, Caoping and Zhashui granitic plutons in the South Qinling orogen. Acta Petrol Sin 25:248–264

Grand'Homme A, Janots E, Seydoux-Guillaume AM, Guillaume D, Bosse V, Magnin V (2017) Partial resetting of the U-Th-Pb systems in experimentally altered monazite: nanoscale evidence of incomplete replacement. Geology 44:431–434

Gregory CJ, Rubatto D, Allen CM, Williams IS, Hermann J, Ireland T (2007) Allanite micro-geochronology: a LA-ICP-MS and SHRIMP U–Th–Pb study. Chem Geol 245:162–182

Harlov DE, Förster HJ (2003) Fluid-induced nucleation of (Y+REE)-phosphate minerals within apatite: nature and experiment. Part II. Fluorapatite. Am Mineral 87:1209–1229

Harlov DE, Wirth R, Förster HJ (2005) An experimental study of dissolution–reprecipitation in fluorapatite: fluid infiltration and the formation of monazite. Contrib Mineral Petrol 150:268–286

Harlov DE, Wirth R, Hetherington CJ (2011) Fluid-mediated partial alteration in monazite: the role of coupled dissolution–reprecipitation in element redistribution and mass transfer. Contrib Mineral Petrol 162:329–348

Huang DH, Wu CY, Du AD, He HL (1995) Re-Os Isotope ages of molybdenum deposits in East Qinling and their significance. Chin J Geochem 14: 313-322.

Huang DH, Hou ZQ, Yang ZM, Li ZQ, Xu DX (2009) Geological and geochemical characteristics, metallogenetic mechanism and tectonic setting of carbonatite vein-type Mo (Pb) deposits in the East Qinling molybdenum ore belt. Acta Geol Sin 83:1968–1984 (in Chinese with English abstract)

Huang XL, Niu Y, Xu YG, Yang QJ, Zhong JW (2010) Geochemistry of TTG and TTG-like gneisses from Lushan-Taihua complex in the southern North China Craton: implications for late Archean crustal accretion. Precambrian Res 182:43–56

Kosler J, Tubrett MN, Sylvester PJ (2010) Application of laser ablation ICP-MS to U-Th-Pb dating of monazite. Geostand Geoanal Res 25: 375–386

Kröner A, Compston W, Zhang GW, Guo AL, Todt W (1988) Age and tectonic setting of Late Archean greenstone-gneiss terrain in Henan Province, China, as revealed by single-grain zircon dating. Geology 16:211–215

Kynicky J, Smith MP, Xu C (2012) Diversity of rare earth deposits: the key example of China. Elements 8:361–367

Li JH (2014) Re-os isotopic dating of molybdenites from the Dashimengou molybdenum deposit in Songxian County, Henan Province, and its geological significance. Geol China 41:1364–1374 (in Chinese with English abstract)

Li N, Pirajno F (2016) Early Mesozoic Mo mineralization in the Qinling Orogen: an overview. Ore Geol Rev 81:431–450

Li SZ, Kusky TM, Wang L, Zhang G, Lai S, Liu X, Dong S, Zhao G (2007) Collision leading to multiple-stage large-scale extrusion in the Qinling orogen: insights from the Mianlue suture. Gondwana Res 12:121–143

Li JH, Yin JW, Chen HK, Zhang TL (2008) Discussion on the genesis of cryptoexplosion breccia and Mo-Au metallization in Pangxiegou of Song county. Uranium Geol 24:85–89 (in Chinese with English abstract)

Li CL, Yu XQ, Liu JL, Wang BY, Chen SQ, Dai YP (2012a) Geochronology of the indosinian Dongjikou pyroxene syenite from Xiaoqinling area and its tectonic implications. J Jilin U 42:1806–1816 (in Chinese with English abstract)

Li HM, Wang DH, Wang XX, Zhang CQ, Li LX (2012b) The early Mesozoic syenogranite in Xiong'er mountain area, south margin of North China craton: SHRIMP zircon U-Pb dating, geochemistry and its significance. Acta Petrol Mineral 31:771–782 (in Chinese with English abstract)

Li JH, Chen H, Zhang H, Zhang Y, Zhang T, Wen G, Zhang P (2017) Mineralization characteristics and ore genesis of the light rare earth deposit in Taiping town, western Henan. Geol China 44:288–300 (in Chinese with English abstract)

Li Y, Liang W, Zhang G, Ran Y, Shen Q, Wang J, Jin C (2018) Granitoid emplacement during syn-convergent transtension: an example from the Huamenlou pluton in north Qinling, Central China. Geosci Front 9:191–205

Ling W, Ren B, Duan R, Liu X, Mao X, Peng L, Liu Z, Cheng J, Yang H (2008) Timing of the Wudangshan, Yaolinghe volcanic sequences and mafic sills in South Qinling: U-Pb zircon geochronology and tectonic implication. Chin Sci Bull 53:2192–2199

Ling X, Li Q, Liu Y, Yang YH, Liu Y, Tang G, Li XH (2016) In-situ SIMS Th–Pb dating of bastnaesite: constraint on the mineralization time of the Himalayan Mianning-Dechang rare earth element deposits. J Anal Atom Spectrom 31:1680–1687

Liu Y, Gao S, Hu Z, Gao C, Zong K, Wang D (2010) Continental and oceanic crust recycling-induced melt–peridotite interactions in the trans-North China Orogen: U–Pb dating, Hf isotopes and trace elements in zircons from mantle xenoliths. J Petrol 51:537–571

Liu L, Liao X, Wang Y, Wang C, Santosh M, Yang M, Zhang C, Chen D (2016) Early Paleozoic tectonic evolution of the North Qinling Orogenic Belt in Central China: insights on continental deep subduction and multiphase exhumation. Earth-Sci Rev 159:58–81

Lu J, Xu C, Ying Y, Chen W (2014) In-situ chemical, isotopic and geochronological investigation of the Shaxiongdong carbonatite complex. Goldschmidt Conference Abstracts, China, p 1897

Ludwig KR (2003) Isoplot v. 3.0: a geochronological toolkit for Microsoft Excel. Berkeley Geochronology Center, Berkeley, CA

Ma C, She Z, Xu P, Wang L (2005) Silurian A-type granitoids in the southern margin of the Tongbai-Dabieshan: evidence from SHRIMP zircon geochronology and geochemistry. Sci China 48: 1134–1145

Mao JW, Pirajno F, Xiang JF, Gao JJ, Ye HS, Li YF, Guo BJ (2011) Mesozoic molybdenum deposits in the east Qinling–Dabie orogenic belt: characteristics and tectonic settings. Ore Geol Rev 43:264–293

Meng QR, Zhang GW (1999) Timing of collision of the North and South China blocks: controversy and reconciliation. Geology 27:123–126

Meng QR, Zhang GW (2000) Geologic framework and tectonic evolution of the Qinling orogen, Central China. Tectonophysics 323:183–196

Paquette JL, Tiepolo M (2007) High resolution (5 μm) U-Th-Pb isotope dating of monazite with excimer laser ablation (ELA)-ICPMS. Chem Geol 240:222–237

Parrish RR (1990) U–Pb dating of monazite and its application to geological problems. Can J Earth Sci 27:1431–1450

Poitrasson F, Chenery S, Shepherd TJ (2000) Electron microprobe and LA-ICP-MS study of monazite hydrothermal alteration: implications for U-Th-Pb geochronology and nuclear ceramics. Geochim Cosmochim Acta 64:3283–3297

Qian DD, Li JQ (1996) The discovering history of Chinese deposits: Hubei volume. Geological Publishing House, Beijing, p 177 (in Chinese)

Qin JF, Lai SC, Li YF (2007) Genesis of the indosinian guangtoushan adakitic biotite plagiogranite in the Mianxian-Lueyang (Mianlue) suture, South Qinling, China, and its tectonic implications. Geol Bull China 26:466–471

Rasmussen B, Muhling JR (2007) Monazite begets monazite: evidence for dissolution of detrital monazite and reprecipitation of syntectonic monazite during low-grade regional metamorphism. Contrib Mineral Petrol 154:675–689

Ratschbacher L, Hacker BR, Calvert A, Webb LE, Grimmer JC, Mcwilliams MO, Ireland T, Dong S, Hu J (2003) Tectonics of the Qinling (Central China): tectonostratigraphy, geochronology, and deformation history. Tectonophysics 366:1–53

Sal'nikova EB, Yakovleva SZ, Nikiforov AV, Kotov AB, Yarmolyuk VV, Anisimova IV, Sugorakova AM, Plotkina YV (2010) Bastnaesite: a promising U-Pb geochronological tool. Dokl Earth Sci 430:134–136

Schärer U (1984) The effect of initial 230Th disequilibrium on young U-Pb ages; the Makalu case, Himalaya. Earth Planet Sci Lett 67:191–204

Simonetti A, Heaman LM, Chacko T, Banerjee NR (2006) In situ petrographic thin section U-Pb dating of zircon, monazite, and titanite laser ablation-MC-ICP-MS. Int J Mass Spectrom 253:87–97

Smith M, Kynicky J, Xu C, Song W, Spratt J, Jeffries T, Brtnicky M, Kopriva A, Cangelosi D (2018) The origin of secondary heavy rare earth element enrichment in carbonatites: constraints from the evolution of the Huanglongpu district, China. Lithos 48:787–789

Song W, Xu C, Qi L, Zhou L, Wang L, Kynicky J (2015) Genesis of Si-rich carbonatites in Huanglongpu Mo deposit, lesser Qinling orogen, China and significance for Mo mineralization. Ore Geol Rev 64: 756–765

Song W, Xu C, Smith MP, Kynicky J, Huang K, Wei C, Zhou L, Shu Q (2016) Origin of unusual HREE-Mo-rich carbonatites in the Qinling orogen, China. Sci Rep-UK 6:1–9

Stacey JS, Kramers JD (1975) Approximation of terrestrial Pb isotope composition by a two-stage model. Earth Planet Sci Lett 26:207–222

Stein H (1997) Highly precise and accurate Re-Os ages for molybdenite from the East Qinling molybdenum belt, Shaanxi Province, China. Econ Geol 92:827–835

Tera F, Wasserburg GJ (1972a) U-Th-Pb systematics in lunar highland samples from the Luna 20 and Apollo 16 missions. Earth Planet Sci Lett 17:36–51

Tera F, Wasserburg GJ (1972b) U-Th-Pb systematics in three Apollo 14 basalts and the problem of initial Pb in lunar rocks. Earth Planet Sci Lett 14:281–304

Wan J, Gao LB, Wang LX (1992) Metallogenic environmental study and prospect assessment of the granite-pegmatite-type uranium deposit in Shangxian-Danfeng triangle area, Shanxi. Uranium Geol 8:257–263 (in Chinese with English abstract)

Wan Y, Wilde SA, Liu D, Yang C, Song B, Yin X (2006) Further evidence for ~1.85 Ga metamorphism in the central zone of the North China craton: SHRIMP U–Pb dating of zircon from metamorphic rocks in the Lushan area, Henan Province. Gondwana Res 9:189–197

Wan J, Liu C, Yang C, Liu W, Li X, Fu X, Liu X (2016) Geochemical characteristics and LA-ICP-MS zircon U-Pb age of the trachytic volcanic rocks in Zhushan area of Southern Qinling Mountains and their significance. Geol Bull China 35:1134–1143 (in Chinese with English abstract)

Wang X, Wang T, Jahn BM, Nenggao HU, Chen W (2007) Tectonic significance of late Triassic post-collisional lamprophyre dikes from the Qinling Mountains, China. Geol Mag 144:837–848

Wang XX, Wang T, Zhang CL (2015) Granitoid magmatism in the Qinling orogen, Central China and its bearing on orogenic evolution. Sci China Earth Sci 58:1497–1512

Wang RR, Xu ZQ, Santosh M, Liang FH, Fu XH (2017) Petrogenesis and tectonic implications of the early Paleozoic intermediate and mafic intrusions in the south Qinling Belt, Central China: constraints from geochemistry, zircon U–Pb geochronology and Hf isotopes. Tectonophysics 712-713:270–288

Wang JC, Kang QQ, Cui HZ, Yuan F, Zhao JF, Sha YZ, Liu JJ, Zhang HY, Wang GW (2018) Ore-controlling factor and exploration direction of granite pegmatite uranium deposit in North Qinling region. Uranium Geol 34:209–215 (in Chinese with English abstract)

Wetherill GW (1956) Discordant uranium-lead ages. Trans Am Geophys Union (AGU) 37:320–326

Williams ML, Jercinovic MJ, Harlov DE, Budzyń B, Hetherington CJ (2011) Resetting monazite ages during fluid-related alteration. Chem Geol 283:218–225

Wu YB, Zheng YF (2013) Tectonic evolution of a composite collision orogen: an overview on the Qinling–Tongbai–Hong'an–Dabie–Sulu orogenic belt in Central China. Gondwana Res 23:1402–1428

Wu CX, Fang X, Yan H (2015) Charactersitcis of niobium, rare earth deposit and prospecting direction of Wudang. Resour Environ Eng 29:270–298 (in Chinese with English abstract)

Xu C, Campbell IH, Allen CM, Chen Y, Huang Z, Qi L, Zhang G, Yan Z (2008) U–Pb zircon age, geochemical and isotopic characteristics of carbonatite and syenite complexes from the Shaxiongdong, China. Lithos 105:118–128

Xu C, Kynicky J, Chakhmouradian AR, Qi L, Song W (2010) A unique Mo deposit associated with carbonatites in the Qinling orogenic belt, Central China. Lithos 118:50–60

Xu XY, Xia LQ, Xia ZC, Huang YH (2013) Geochemical characteristics and petrogenesis of the early Paleozoic akali lamprophyre complex from Langao County. Acta Geol Sin 22:55–60 (in Chinese with English abstract)

Xu C, Chakhmouradian AR, Taylor RN, Kynicky J, Li W, Song W, Fletcher IR (2014) Origin of carbonatites in the south Qinling orogen: implications for crustal recycling and timing of collision between the south and North China blocks. Geochim Cosmochim Acta 143:189–206

Xu C, Kynicky J, Chakhmouradian AR, Li X, Song W (2015) A case example of the importance of multi-analytical approach in

deciphering carbonatite petrogenesis in South Qinling orogen: Miaoya rare-metal deposit, central China. Lithos 227:107–121

Yang YH, Wu FY, Li R, Yang JH, Xie LW, Liu Y, Zhang YB, Huang C (2014) In situ U-Pb dating of bastnaesite by LA-ICPMS. J Anal Atom Spectrom 29:1017–1023

Ying Y, Chen W, Lu J, Jiang SY, Yang Y, Ying Y, Chen W, Lu J, Jiang SY, Yang Y (2017) In situ U-Th-Pb ages of the Miaoya carbonatite complex in the South Qinling orogenic belt, Central China. Lithos 290:159–171

Yuan F, Liu J, Guxian L, Sha Y, Zhang S, Zhai D, Wang G, Zhang H, Liu G, Yang S (2017) Zircon U-Pb geochronology, geochemistry and petrogenesis of the granites and pegmatites from the Guangshigou uranium deposit in the northern Qinling Orogen,China. Geosci Front 24:25–45 (in Chinese with English abstract)

Yuan F, Liu J, Carranza EJM, Zhang S, Zhai DG, Liu G, Wang WG, Zhang HY, Sha YZ, Yang SS (2018) Zircon trace element and isotopic (Sr, Nd, Hf, Pb) effects of assimilation-fractional crystallization of pegmatite magma: a case study of the Guangshigou biotite pegmatites from the north Qinling Orogen, Central China. Lithos 302-303:20–36

Zhang ZQ, Liu DY, Fu GM (1994) Isotopic geochronology of metamorphic strata in north Qinling. Geological Publishing House, Beijing China, p 191 (in Chinese)

Zhang GW, Zhang BR, Yuan XC, Xiao QH (2001a) Qingling Orogenic Belt and continent dynamics. Science Press, Beijing, p 855 (in Chinese)

Zhang L, Wang LS, Zhou L (2001b) Subduction of back-arc basin and recycling of crustal substance in northern Qinling: geochemical evidence of Taoyuan intrusion and Huanggang intrusive complex. Earth Sci-J China Univ Geosci 26:18–24 (in Chinese with English abstract)

Zhang CL, Gao S, Yuan HL, Zhang GW, Yan YX, Luo JL, Luo JH (2007) Sr-Nd-Pb isotopes of the early Paleozoic mafic-ultramafic dykes and basalts from south Qinling belt and their implications for mantle composition. Sci China Earth Sci 50:1293–1301

Zhang CL, Liu L, Wang T, Wang XX, Li L, Gong QF, Li XF (2013) Granitic magmatism related to early Paleozoic continental collision in north Qinling. Chin Sci Bull 58:4405–4410

Zhao T, Zhai M, Xia B, Huimin LI, Zhang Y, Wan Y (2004) Zircon U-Pb SHRIMP dating for the volcanic rocks of the Xiong'er group: constraints on the initial formation age of the cover of the North China craton. Chin Sci Bull 49:2495–2502

Zhao G, He Y, Sun M (2009) The Xiong'er volcanic belt at the southern margin of the North China craton: petrographic and geochemical evidence for its outboard position in the Paleo-Mesoproterozoic Columbia supercontinent. Gondwana Res 16:170–181

Zhu X, Chen F, Nie H, Siebel W, Yang Y, Xue Y, Zhai M (2014) Neoproterozoic tectonic evolution of South Qinling, China: evidence from zircon ages and geochemistry of the Yaolinghe volcanic rocks. Precambrian Res 245:115–130

Zhu HQ, Li WH, Hui ZP, Zhao RY, Wang JB, Gong QF (2015) Mineralization characteristics and metallogenesis of granitic pegmatite uranium and ther Rare Metals in the Danfeng triangle area, Shaanxi. Northwest Geol 48:172–178 (in Chinese with English abstract)

Zhu J, Wang L, Peng S, Peng L, Wu C, Qiu X (2016) U-Pb zircon age, geochemical and isotopic characteristics of the Miaoya syenite and carbonatite complex, Central China. Geol J 52:938–954

Zhu J, Cheng CH, Wang LX, Peng SG, Peng LH, Ke X (2017) Some new knowledge concerning Silurian alkaline magmatism and related Nb-REE mineralization in the Zhushan region, South Qinling. Acta Petrol Min 29:681–690 (in Chinese with English abstract)